

High-Fidelity, Low-Loss State Detection of Alkali-Metal Atoms in Optical Tweezer Traps

Matthew N. H. Chow,^{1,2,3,*} Bethany J. Little,¹ and Yuan-Yu Jau^{1,2,3}

¹Sandia National Laboratories, Albuquerque, New Mexico 87185, USA

²Department of Physics and Astronomy, University of New Mexico, Albuquerque, New Mexico 87106, USA

³Center for Quantum Information and Control, University of New Mexico, Albuquerque, New Mexico 87131, USA

(Dated: August 15, 2022)

We demonstrate discrimination of ground-state hyperfine manifolds of a cesium atom in an optical tweezer using a simple probe beam with $99.91^{+0.02}_{-0.02}\%$ detection fidelity and $0.9(2)\%$ detection-driven loss of bright state atoms. Our detection infidelity of $0.09^{+0.02}_{-0.02}\%$ is an order of magnitude better than previously published low-loss readout results for alkali-metal atoms in optical tweezers. Our low atom loss and high-fidelity state detection eliminates the extra depumping mechanism due to population transfer between excited-state sublevels through V-type stimulated Raman transitions caused by the trap laser when the probe laser is present. In this work, complex optical systems and stringent vacuum pressures are not required.

Neutral atoms in arrays of optical dipole traps (ODTs) provide a promising platform for quantum computing [1–3], quantum simulation [4, 5], quantum chemistry [6], and optical clocks [7]. Atoms can be individually controlled inside tightly focused beams, known as optical tweezers, and have been used to generate defect-free arrays of tens to hundreds of atoms in one-, two- and three-dimensional geometries [8–11]. Alkali-metal atoms are frequently utilized because of the simplicity of their electronic structure and well-established methods of laser cooling [12].

Performance of alkali-metal atoms in tweezer platforms has to date been limited by state readout fidelity. Detection schemes are typically based on either state-dependent fluorescence collection or loss, where the state of the atom is mapped to trap occupation. Although relatively high detection fidelity has been achieved with loss-based schemes [3], these methods impose a vacuum-dependent upper bound on readout fidelity, slow the repetition rate, and complicate algorithms requiring mid-circuit measurement. Fluorescence detection on the other hand allows – in principle – for high fidelity state measurement without losing the atom. Previously,

results for alkali atoms with fluorescence detection have only shown $>1.2\%$ infidelity without enhancement from an optical cavity [13–18]. Alternately, high-fidelity, low-loss detection of alkali atoms has been demonstrated in an optical lattice using a state-dependent potential method [19], but adaptation of this method to optical tweezers is not straightforward.

In this paper, we report state discrimination between ground-state hyperfine manifolds of Cs atoms with $0.09^{+0.02}_{-0.02}\%$ infidelity while suffering only $0.9(2)\%$ detection-driven losses of the bright state. We achieve these results by implementing an adaptive detection scheme to manage detection heating and mitigating a previously unreported state information loss channel stemming from simultaneous probe and trap illumination. We do not impose any stringent vacuum or optical system requirements to achieve this result, enabling straightforward integration of our techniques on contemporary alkali-metal atom tweezer platforms.

This work is an important step towards scalable, high performance alkali-tweezer machines. While the measurement error on noisy intermediate-scale quantum (NISQ) computers is often overlooked as it does not typically scale with algorithm length, it is important to consider the (generally exponential) scaling of the measurement error with system size. In addition, by demonstrating simultaneous high-fidelity and low loss, we improve the outlook for quantum sensing applications where the sensitivity is tied to atom retention capability via repetition rate.

Our experimental sequence is triggered upon loading a Cs atom from a magneto-optical trap into a tweezer trap. The tweezer is formed by focusing up to 10 mW of linearly polarized 937 nm laser light through a 0.45 NA microscope objective to a spot with a $1.6\mu\text{m}/e^2$ waist radius. The trap is small enough that a light-assisted collisional-blockade mechanism ensures loading no more than one atom at a time [20]. The trap wavelength of $\lambda_{\text{trap}} = 937\text{ nm}$ is chosen to be red-detuned from both the D_1 and D_2 line transitions and to have approximately the same AC Stark shift on both states ($6S_{1/2}$ and $6P_{3/2}$) of the cooling transition (*i.e.* “magic”). After loading an atom, we cool it with polarization-gradient cooling to $\approx 2\mu\text{K}$. The atom is then prepared in either $|F = 4\rangle$ (“bright”) or $|F = 3\rangle$ (“dark”) hyperfine ground manifolds and the state

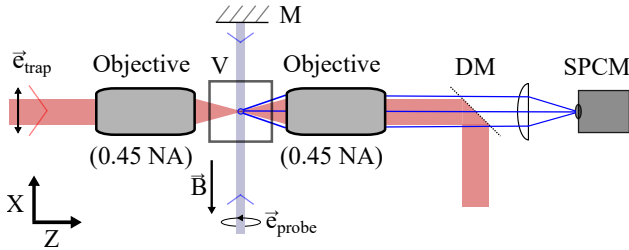


FIG. 1: We use a simple probe beam and fluorescence collection optical system to measure high-fidelity state detection. Both the probe beam (blue shaded line) propagation direction and trap light (red shaded line) polarization (\vec{e}_{trap}) are oriented along the bias magnetic field direction (\vec{B}). The probe is left-hand circularly polarized in order to drive only σ_+ transitions. The probe is retroreflected with a gold mirror (M) to minimize polarization distortions. Fluorescence (blue rays) is collected outside of the vacuum chamber (V) with a 0.45 NA microscope objective, separated from the trap light with a dichroic mirror (DM), and focused onto a single-photon counting module (SPCM).

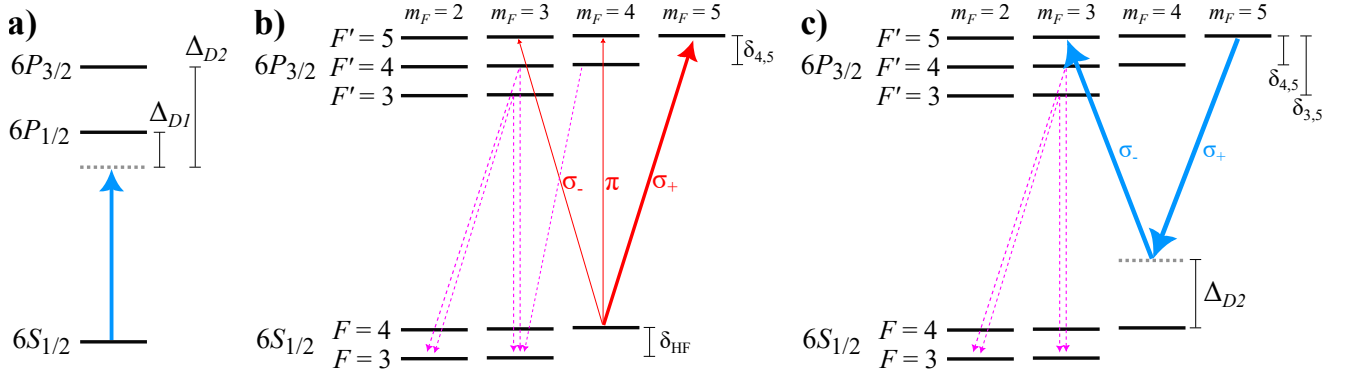


FIG. 2: Three mechanisms contribute to state information loss during detection. (a) The fundamental limitation of T_1 coherence in an optical dipole trap is imposed by the off-resonant scattering rate of the light used to generate the trapping potential. For trapping parameters used in this manuscript ($U_0 = 8.9(2)$ MHz), T_1 is measured to be $0.49(3)$ s. (b) Probe (solid red lines) polarization impurities and misalignment to the magnetic field axis allow for weak, off-resonant coupling to $F' \neq 5$ excited state hyperfine manifolds, which then have dipole allowed decay channels (dashed lines) to the $F=3$ ground state manifold. (c) σ_{\pm} trap light (solid blue lines) allows for detuned, two-photon coupling from $F'=5$ to $F' \neq 5$ excited state hyperfine manifolds. This depumping mechanism can be effectively eliminated by using π -polarized trap light, for which coupling between $F' = 5, m_F' = 5$ and the lower ground state is not supported. Levels not drawn to scale.

of the atom is then read out using a near-resonant probe laser. Finally, we check for atom retention in the trap with the cooling beams.

During detection, we use a near resonant probe beam that is tuned to the $F=4$ to $F'=5$ D_2 line transition so the $F=4$, bright ground state scatters probe photons in a closed cycling transition, while the $F=3$ state is dark to the probe and ideally scatters no light. State-dependent fluorescence is then collected and imaged onto a single photon counting module (SPCM), which is monitored in real time by our field programmable gate-array (FPGA) control system. The atom is assigned a label, bright or dark, based on a discrimination threshold level of collected photon counts. The probe beam is left-hand circularly polarized and a bias magnetic field (B-field) of 4 G is set counter to its propagation direction such that we drive primarily σ_+ transitions. Thus, we quickly pump the atom into the $F = 4, m_F = 4$ “stretched” ground state, which is protected via angular momentum conservation against depumping to the dark state through off-resonant coupling to $F' \neq 5$ states. There is also a small, transient probability of depumping during the driven random walk up to the stretched state if the atom is initialized in a different Zeeman state - see Ref. [14]. For this reason, we turn on the probe beam alongside the repump beam in the last $10 \mu\text{s}$ of optical pumping when preparing the bright state, effectively preparing the stretched state. [21]

In an ideal scenario, we would be able to determine the state of the atom with arbitrary accuracy by collecting scattered photons until the bright and dark count distributions are sufficiently separated. However, recoil heating of the bright state during detection limits the maximum possible probe time before atom loss, and depumping from trap and probe light can lead to state information loss during detection. We study three depumping mechanisms, illustrated in Figure 2: (a) off-

resonant scatter of trap light, (b) probe polarization components that allow for off-resonant scatter to $F' \neq 5$, and (c) trap-induced two-photon coupling of excited state hyperfine manifolds via stimulated Raman transitions. The first mechanism is the main fundamental constraint, and can be mitigated by improving the ratio of photon collection to trap off-resonant scattering rates. The second mechanism is imposed by probe misalignment and polarization impurity, and can be improved with further technical capability. The third is an almost entirely geometrical problem and can be essentially eliminated by an appropriate choice of trap polarization, bias fields, probe polarization, and probe propagation direction. To our knowledge, this third information loss channel has not been previously reported for this type of detection, and mitigation of this depumping pathway turned out to be critical to achieving the state discrimination fidelity observed here.

To guide our choice of detection parameters, we use a statistical model of photon collection governed by the rates of three processes: the count collection rate from a bright atom, the dark collection rate (background), and the rate of state-information loss from the prepared state of the atom (the depump rate). We use a short detection time compared to the depump rate and thus consider at most a single state change event during detection [22]. The resulting photon collection distribution is found by marginalizing over state change event times, t :

$$P(n) = e^{-t_d R_{\text{dep}}} \mathcal{P}(n, R_p t_d) + \int_0^{t_d} \mathcal{P}(n, R_p t + R_{np}(t_d - t)) R_{\text{dep}} e^{-t R_{\text{dep}}} dt. \quad (1)$$

Here, $P(n)$ is the probability of detecting n photons, $\mathcal{P}(n, Rt) = e^{-Rt} (Rt)^n / n!$ is probability of n events in a Poisson distribution of mean Rt , t_d is the total detection time, R_p is the

photon collection rate from an atom in the prepared state, R_{np} is the collection rate from the atom after a state changing event (i.e., collection rate from the non-prepared state), and R_{dep} is the depumping rate out of the prepared state. The first term represents the contribution from cases where no depumping occurs, and the second term is the convolution of counts from before and after a state change event that occurs during the detection window.

Thresholding at m detected counts to assign state labels, we define the bright label probability as a function of F , the prepared state: $P_{\text{bright}}(F) = \sum_{n=m}^{\infty} P(n|F)$. The bright state readout error is the probability of failing to assign a bright label to an atom prepared in the bright state: $\epsilon_{\text{bright}} = 1 - P_{\text{bright}}(F = 4)$, and similarly the dark state readout error is the probability of assigning a bright label to an atom prepared in the dark state: $\epsilon_{\text{dark}} = P_{\text{bright}}(F = 3)$. For all infidelities quoted in this work, we use $\mathcal{I} = \frac{1}{2}(\epsilon_{\text{bright}} + \epsilon_{\text{dark}})$, and all fidelities are $\mathcal{F} = 1 - \mathcal{I}$. Numerically, we find that the optimal threshold level is $m = 3$ counts to discriminate between bright and dark in the range of collection and depumping rates near our experiment parameters.

The background photon collection rate is $5.2(3) \times 10^2 \text{ s}^{-1}$ and the bright atom collection rate is $5.44(3) \times 10^4 \text{ s}^{-1}$, such that optimal error rates of $\epsilon_{\text{bright}} = 0.005\%$ and $\epsilon_{\text{dark}} = 0.04\%$ would be achieved in an ideal, depump-free, case at 0.26 ms of probe time. However, observed error rates are significantly higher (especially for the bright state), indicating that state information loss during detection is the dominant source of detection infidelity. As a figure of merit, we consider the rate of information loss, R_{dep} , compared to the rate of information gain, R_{bright} : $\mathcal{R} = R_{\text{dep}}/R_{\text{bright}}$. \mathcal{R} is the depump probability per collection event of the bright state. As a rough approximation for estimating fidelity, one can consider the probability of collecting m photons from the bright state prior to depump, $(1 - \mathcal{R})^m \approx 1 - m\mathcal{R}$ for $m\mathcal{R} \ll 1$.

We begin our analysis of state information loss during detection by considering single photon off-resonant scattering from the trapping laser, illustrated in Fig. 2a. Using a numeric density matrix model including all magnetic levels of the ground and first excited states ($6P_{1/2}$ & $6P_{3/2}$), we find that the depumping rate from the trap light is $R_{\text{dep,trap}} \approx 2.5 \times 10^{-7} U_0/h$ [23]. For a trap depth of $U_0/h = 8.9(2) \text{ MHz}$, this yields an effective $T_1 = 1/R_{\text{dep,trap}}$ of 0.45 s and a normalized depump rate of $\mathcal{R}_{\text{trap}} = 4.1 \times 10^{-5}$. To experimentally verify, we measure exponential decay times for the bright (dark) state and find 0.41(3) s (0.58(3) s).

The probe beam may also cause state information loss due to off-resonant scatter, as illustrated in Fig. 2b. Although we attempt to drive only σ_+ transitions with the probe beam, polarization impurity or misalignment of the probe propagation direction to the B-field allows for off-resonant scatter to $F' \neq 5$ levels. Following the calculation in Ref. [14], we find the depump rate by summing over all dipole allowed transition scattering rates, weighted by the branching ratio (b_α) of the excited state ($|\alpha\rangle$) to the $F=3$ ground state manifold [24]. The sum depends on probe polarization purity, alignment to

the B-field, and intensity. Our measured probe polarization purity is 98.5% before entering the vacuum chamber, and we align the B-field by scanning shim fields and maximizing the bright label probability for $F = 4$ after a conservatively long detection time, such that we expect an alignment tolerance of a few degrees and a resulting σ_- - and π -polarization intensity fractions of $\leq 10\%$. This corresponds to a probe off-resonant scatter rate of $\leq 5 \text{ s}^{-1}$, or $\mathcal{R}_{\text{probe}} \leq 9 \times 10^{-5}$; comparable to the depump probability due to the trap off resonant scatter.

Initially our measured depump rate was higher than we would expect from trap and probe off-resonant scatter mechanisms, which prompted investigation of a third mechanism. A trap-light driven, detuned, two-photon effect, shown in Fig. 2c, provides another pathway for atoms to escape the cycling transition subspace. While the ground state hyperfine splitting of $\approx 9.2 \text{ GHz}$ is sufficiently large to prevent significant Λ -type Raman transitions, the excited state hyperfine splitting is only of order 100 MHz. For some choices of experiment geometry, this leads to appreciable population leakage of excited state atoms to $F' \neq 5$ by detuned V-type Raman transitions.

As a case study for this V-type Raman mechanism, we calculate the two-photon depumping rate when the bias B-field is aligned orthogonal to the (linear) trap polarization direction, producing $(\sigma_+ + \sigma_-)/\sqrt{2}$ trap light in the atom's angular momentum basis. Using three-level calculations and a far-detuned approximation [24], we estimate the effective two-photon Rabi rate for the Raman transition from $|F' = 5, m'_F = 5\rangle$ to $|F' = 4(3), m'_F = 3\rangle$ to be $\Omega_{5',4'} = 2.53 \times U_0/h$ ($\Omega_{5',3'} = 4.22 \times U_0/h$). Considering the branching ratio of each state to the $|F = 3\rangle$ ground state, this gives a depump probability per resonant scattering event of 6×10^{-6} , or a normalized depump rate of $\mathcal{R}_\sigma = 6 \times 10^{-4}$ after accounting for our measured collection efficiency (CE) of 0.96(1)% [25]. Since this value is an order of magnitude larger than both the probe and trap single photon off-resonant depumping rates, mitigation of this mechanism yields significant gains for the bright state readout fidelity.

To verify this newly identified mechanism, we study the bright state count histogram for two experiment geometries. We orient the B-field and probe jointly defined quantization axis either parallel or orthogonal to the trap polarization generating either π or σ_\pm polarization components of the trapping beam [26]. With the σ -polarized trap light, we expect to see depumping from the two-photon pathway as calculated, however for the π -polarized trap configuration, there is no dipole-allowed coupling from the excited state to the ground state caused by the trap light, and thus we expect this mechanism to be absent (barring trap polarization misalignment and polarization distortion effects from focusing).

As shown in Fig. 3, when we run the experiment in these two configurations, we find that the histogram of collected light from a bright atom in a π -polarized trap is significantly closer to the ideal depump-free Poisson distribution than that of an atom in a σ -polarized trap. A fit to Eq. (1) yields depumping probabilities per scattering event of $50(5) \times 10^{-6}$

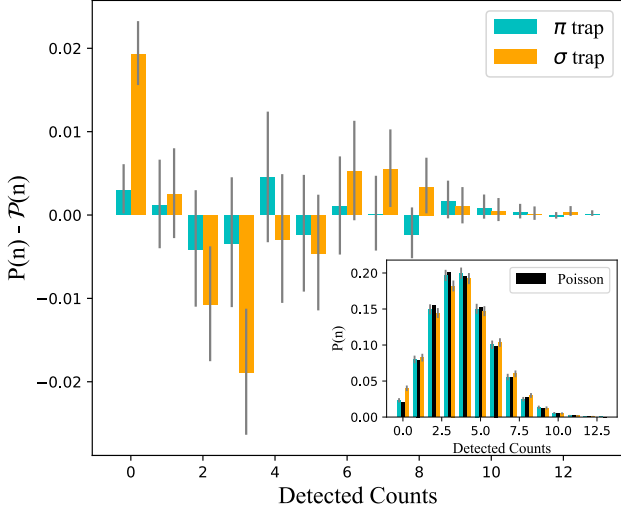


FIG. 3: Bright state detection count histograms for different experiment geometries demonstrate the effect of two-photon depumping from the trap light. In the main figure, we take the difference of detection count histograms for a fixed probe duration, $P(n)$, and the depump-free case of a Poisson distribution with the same mean, $\mathcal{P}(n)$. Full histograms are shown in the inset. The distribution collected using the σ -polarized configuration (orange bars) is both significantly non-Poissonian and has a substantially larger zero bin than that of the π -polarized configuration (teal bars), indicating a higher depump rate in the π -polarized configuration that we attribute to V-type Raman transitions from the trap light. When the trap has σ_{\pm} components, two-photon coupling between excited state hyperfine states through the $F = 4, m_F = 4$ ground state allows for leakage out of the cycling transition manifold, while in the π -polarized trap configuration, the lack of dipole allowed coupling from the $F' = 5, m_F' = 5$ excited state to $F = 4, m_F = 4$ ground state prevents two-photon leakage during bright state detection. There are 10,000 shots in each data histogram; uncertainty markers are Wilson score intervals.

and $7(4) \times 10^{-6}$ for the σ and π configurations respectively. Since the other probe and trap parameters are held fixed, we attribute the difference in the depump rates between the two configurations to off-resonant, V-type Raman transitions. This data was taken prior to a significant optimization of the probe beam optics (alignment and beam quality), and we attribute the remaining depump rate in the π configuration mostly to probe impurities.

Achieving excellent state readout fidelity is crucial for this platform; however, from a practical standpoint atom retention is equally important, and can be a challenging problem to solve. Photon recoil during detection of a bright state atom leads to heating that can easily overcome the trap depth [27, 28]. To this end, we use a counterpropagating probe beam and implement an adaptive detection scheme where we apply our probe laser in a series of $5 \mu s$ pulses until either the threshold level of photons is collected or we reach our maxi-

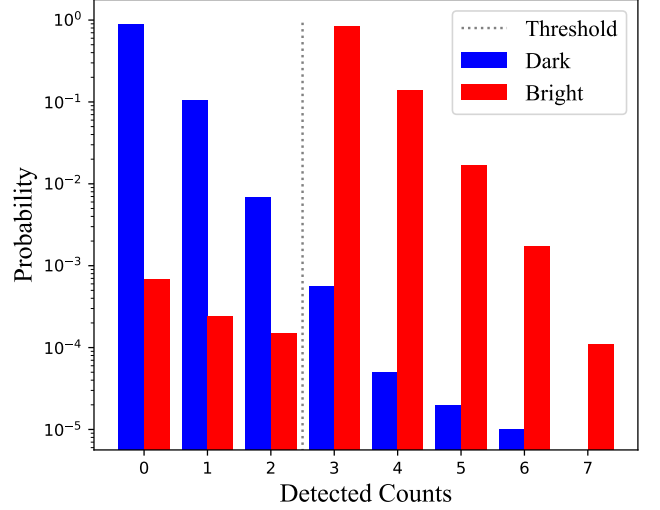


FIG. 4: The normalized histogram of collected photons from the bright and dark state demonstrates $0.09^{+0.02}_{-0.02}\%$ detection infidelity. Single atoms are prepared in either the dark (blue) or bright (red) state and read out by illuminating the atom with the D_2 line probe and collecting scattered photons. When three or more photons are collected, the atom is labelled bright; when fewer than three photons are collected, the atom is labelled dark. Atoms prepared in the bright state are erroneously labelled dark in $0.11^{+0.03}_{-0.02}\%$ of experiments, and atoms prepared in the dark state are erroneously labelled bright in $0.06^{+0.01}_{-0.02}\%$ of experiments. Data presented in this histogram was collected in 1,000 batches of 100 shots, alternating between dark and bright state preparation, for a total of 100,000 shots for each state.

mum probe duration [29–34]. Since extra photons beyond the threshold level provide no additional information in a thresholding detection scheme, this effectively eliminates extraneous heating at no cost to the state discrimination fidelity [24].

We measure our detection fidelity by alternately preparing the atom in each state 100,000 times and recording the number of times that the measured state matches the prepared state, see Fig. 4. We collect the data in 1,000 batches of 100 shots, alternating between bright and dark state preparation for each batch. A total of 107 trials where the atom was prepared in the bright state were read out as dark and 64 trials where the atom was prepared in the dark state were labelled bright, giving a bright error of $\epsilon_{\text{bright}} = 0.11^{+0.03}_{-0.02}\%$ and a dark error of $\epsilon_{\text{dark}} = 0.06^{+0.01}_{-0.02}\%$. This yields an infidelity of $0.09^{+0.02}_{-0.02}\%$, or a fidelity of $99.91^{+0.02}_{-0.02}\%$. Uncertainties given here are Wilson score intervals. This measurement does not correct for state preparation errors, although we expect our state preparation error to be small compared to the readout error. We then infer the detection-driven loss probability by subtracting the ratio of the probability of passing the presence check when preparing in the bright and dark state from unity, and find $0.9(2)\%$ loss of the bright state due to detection.

To test the applicability of our result to atom-array imaging, we also measure the detection fidelity and detection-driven

loss of the bright state without using adaptive detection, which would be challenging using a typical camera due to slow data transfer and processing times. We reduce the probe intensity and use a probe time of $350\text{ }\mu\text{s}$ to achieve a bright error of $\epsilon_{\text{bright}} = 0.22^{+0.03}_{-0.03}\%$ and a dark error of $\epsilon_{\text{dark}} = 0.13^{+0.02}_{-0.02}\%$ for a combined readout infidelity of $0.18^{+0.02}_{-0.02}\%$. We observe an additional 1.8(3)% loss of the bright state [24]. We note that development and integration of single-photon avalanche diode (SPAD) array sensors could potentially provide a suitably fast signal to perform adaptive detection on an array of atoms [35–39]. [40]

Casting the bright state readout error as the total depump probability per collection event, we find $\mathcal{R} = 1 - \sqrt[3]{1 - \epsilon_{\text{bright}}} = 3.7 \times 10^{-4}$. This value is the same order of magnitude as the sum of estimated contributions from off-resonant scatter from probe and trap light. The source of any remaining discrepancy in the observed depump rate is a subject of ongoing study. Possible sources of contribution to observed error rates include imperfect state preparation, overestimation of probe alignment or purity, failed presence checks resulting in poor quality post-selection, and residual σ -polarized components of the trap light due to misalignment of the trap polarization direction to the B-field or polarization distortion effects due to focusing of the trap beam.

This depump rate is sufficiently low to permit high-fidelity detection even in the case of low collection efficiency optical systems. When we fiber-couple our atomic fluorescence, we still achieve $99.84^{+0.02}_{-0.03}\%$ fidelity and 2.6(2)% loss of the bright state, even though the collection efficiency is only 0.37%. In such a system with low depump rates and low collection efficiency, detection heating losses play a more dominant role. We find that, to some degree, we can trade atom survival probability for detection fidelity and reach a detection fidelity of $99.89^{+0.02}_{-0.02}\%$ with 14.1(3)% loss of the bright state due to detection.

We note that further improvement of the detection fidelity and atom retention should be achievable by improving the photon collection efficiency. Our measured collection efficiency of 0.96(1)% is relatively poor compared to other works [14, 15] and we expect that the detection infidelity should improve approximately linearly with the ratio of collected photons to depump rate. We also note that these results ease vacuum system requirements for high fidelity detection of alkali atoms in optical tweezers, since detection fidelity is independent of the background atom loss rate. To achieve comparable fidelities with a push out method, the average atom loss rate due to background gas collisions (or indeed any source other than the pushout beam) must be comparable to the readout error reported here, since a dark atom lost due to background is indistinguishable from a bright atom lost to the pushout beam in such schemes. Finally, we note that our result obviates the need for toggling the trap and probe beams, as we keep the trap beam on at all times and still achieve high fidelity. Use of a magic wavelength trap is important for our ability to keep the trap on, as we avoid dipole force fluctuation (DFF) heating [27]. Toggling the trap and probe beam could be an alternate

strategy to mitigate both the two-photon depumping mechanism and DFF heating, at the cost of potentially introducing an extra heating mechanism from repeated kicks.

Ultimately, the fidelity reported here is the result of study of the relevant atom-photon interaction physics, and mitigation of a previously unreported depumping mechanism under simultaneous trap and probe illumination. We find that the remaining infidelity from off-resonant scattering of trap and probe light is sufficiently low to enable an order of magnitude improvement over previously published low-loss readout of alkali atoms in optical tweezers. In conjunction with the high atom retention enabled by adaptive detection, this result alludes to promise of near-term detection suitable for fault tolerant operation and the possibility of non-disruptive mid circuit measurement for error detecting or correcting algorithms. This work represents an important step towards building scalable, high-performance quantum information processors and quantum sensors out of alkali-metal atoms trapped in optical tweezers.

We thank Ivan Deutsch, Vikas Buchemmavari, Justin Schultz, and Paul Parazzoli for helpful discussions. Sandia National Laboratories is a multimission laboratory managed and operated by National Technology & Engineering Solutions of Sandia, LLC, a wholly owned subsidiary of Honeywell International Inc., for the U.S. Department of Energy's National Nuclear Security Administration under contract DE-NA0003525. This paper describes objective technical results and analysis. Any subjective views or opinions that might be expressed in the paper do not necessarily represent the views of the U.S. Department of Energy or the United States Government. SAND2022-10823 O

* mnchow@sandia.gov

- [1] I. S. Madjarov, J. P. Covey, A. L. Shaw, J. Choi, A. Kale, A. Cooper, H. Pichler, V. Schkolnik, J. R. Williams, and M. Endres, *Nature Physics* **16**, 857 (2020).
- [2] H. Levine, A. Keesling, G. Semeghini, A. Omran, T. T. Wang, S. Ebadi, H. Bernien, M. Greiner, V. Vuletić, H. Pichler, and M. D. Lukin, *Phys. Rev. Lett.* **123**, 170503 (2019).
- [3] D. Bluvstein, H. Levine, G. Semeghini, T. T. Wang, S. Ebadi, M. Kalinowski, A. Keesling, N. Maskara, H. Pichler, M. Greiner, V. Vuletić, and M. D. Lukin, *Nature* **604**, 451 (2022).
- [4] H. Bernien, S. Schwartz, A. Keesling, H. Levine, A. Omran, H. Pichler, S. Choi, A. S. Zibrov, M. Endres, M. Greiner, V. Vuletić, and M. D. Lukin, *Nature* **551**, 579 (2017).
- [5] H. Labuhn, D. Barredo, S. Ravets, S. de Léséleuc, T. Macrì, T. Lahaye, and A. Browaeys, *Nature* **534**, 667 (2016).
- [6] J. T. Zhang, Y. Yu, W. B. Cairncross, K. Wang, L. R. B. Picard, J. D. Hood, Y.-W. Lin, J. M. Hutson, and K.-K. Ni, *Phys. Rev. Lett.* **124**, 253401 (2020).
- [7] A. W. Young, W. J. Eckner, W. R. Milner, D. Kedar, M. A. Norcia, E. Oelker, N. Schine, J. Ye, and A. M. Kaufman, *Nature* **588**, 408 (2020).
- [8] M. Endres, H. Bernien, A. Keesling, H. Levine, E. R. Anschuetz, A. Krajenbrink, C. Senko, V. Vuletic,

- M. Greiner, and M. D. Lukin, *Science* **354**, 1024 (2016), <https://www.science.org/doi/pdf/10.1126/science.aah3752>.
- [9] D. Barredo, S. de Léséleuc, V. Lienhard, T. Lahaye, and A. Browaeys, *Science* **354**, 1021 (2016), <https://www.science.org/doi/pdf/10.1126/science.aah3778>.
- [10] D. Ohl de Mello, D. Schaffner, J. Werkmann, T. Preuschoff, L. Kohfahl, M. Schlosser, and G. Birkel, *Phys. Rev. Lett.* **122**, 203601 (2019).
- [11] D. Barredo, V. Lienhard, S. de Léséleuc, T. Lahaye, and A. Browaeys, *Nature* **561**, 79 (2018).
- [12] Alkaline earth and Helium-like atoms have become an increasingly popular choice as well, with the most recent progress in Strontium and Ytterbium, which have attractive, narrow line optical clock transitions.
- [13] A. Fuhrmanek, R. Bourgain, Y. R. P. Sortais, and A. Browaeys, *Phys. Rev. Lett.* **106**, 133003 (2011).
- [14] M. Kwon, M. F. Ebert, T. G. Walker, and M. Saffman, *Phys. Rev. Lett.* **119**, 180504 (2017).
- [15] M. Martinez-Dorantes, W. Alt, J. Gallego, S. Ghosh, L. Ratschbacher, Y. Völzke, and D. Meschede, *Phys. Rev. Lett.* **119**, 180503 (2017).
- [16] J. Bochmann, M. Mücke, C. Guhl, S. Ritter, G. Rempe, and D. L. Moehring, *Phys. Rev. Lett.* **104**, 203601 (2010).
- [17] R. Gehr, J. Volz, G. Dubois, T. Steinmetz, Y. Colombe, B. L. Lev, R. Long, J. Estève, and J. Reichel, *Phys. Rev. Lett.* **104**, 203602 (2010).
- [18] E. Deist, Y.-H. Lu, J. Ho, M. K. Pasha, J. Zeiher, Z. Yan, and D. M. Stamper-Kurn, Fast non-destructive cavity readout of single atoms within a coherent atom array (2022).
- [19] T.-Y. Wu, A. Kumar, F. Giraldo, and D. S. Weiss, *Nature Physics* **15**, 538 (2019).
- [20] T. Grünzweig, A. Hilliard, M. McGovern, and M. F. Andersen, *Nature Physics* **6**, 951 (2010).
- [21] We also retroreflect the probe beam to balance the recoil force and use a gold mirror to minimize polarization distortion.
- [22] We initially considered the possibility of multiple state change events, however that is suppressed to first order in $t_d R_{dep}$.
- [23] W. Happer, Y.-Y. Jau, and T. Walker, *Optically Pumped Atoms* (Wiley-VCH, Weinheim, 2010).
- [24] Supplemental material in preparation.
- [25] Collection efficiency quoted here includes transmission through all optics and the quantum efficiency of the detector.
- [26] Neglecting polarization distortion due to focusing and incorrect polarization components due to misalignment.
- [27] M. Martinez-Dorantes, W. Alt, J. Gallego, S. Ghosh, L. Ratschbacher, and D. Meschede, *Phys. Rev. A* **97**, 023410 (2018).
- [28] D. J. Wineland and W. M. Itano, *Phys. Rev. A* **20**, 1521 (1979).
- [29] M. J. Gibbons, C. D. Hamley, C.-Y. Shih, and M. S. Chapman, *Phys. Rev. Lett.* **106**, 133002 (2011).
- [30] D. B. Hume, T. Rosenband, and D. J. Wineland, *Phys. Rev. Lett.* **99**, 120502 (2007).
- [31] A. H. Myerson, D. J. Szwer, S. C. Webster, D. T. C. Allcock, M. J. Curtis, G. Imreh, J. A. Sherman, D. N. Stacey, A. M. Steane, and D. M. Lucas, *Phys. Rev. Lett.* **100**, 200502 (2008).
- [32] S. D. Erickson, J. J. Wu, P.-Y. Hou, D. C. Cole, S. Geller, A. Kwiatkowski, S. Glancy, E. Knill, D. H. Slichter, A. C. Wilson, and D. Leibfried, *Phys. Rev. Lett.* **128**, 160503 (2022).
- [33] S. Crain, C. Cahall, G. Vrijsen, E. E. Wollman, M. D. Shaw, V. B. Verma, S. W. Nam, and J. Kim, *Communications Physics* **2**, 97 (2019).
- [34] S. L. Todaro, V. B. Verma, K. C. McCormick, D. T. C. Allcock, R. P. Mirin, D. J. Wineland, S. W. Nam, A. C. Wilson, D. Leibfried, and D. H. Slichter, *Phys. Rev. Lett.* **126**, 010501 (2021).
- [35] N. A. W. Dutton, I. Gyongy, L. Parmesan, S. Gnechchi, N. Calder, B. R. Rae, S. Pellegrini, L. A. Grant, and R. K. Henderson, *IEEE Transactions on Electron Devices* **63**, 189 (2016).
- [36] M. Gersbach, J. Richardson, E. Mazaleyrat, S. Hardillier, C. Niclass, R. Henderson, L. Grant, and E. Charbon, *Solid-State Electronics* **53**, 803 (2009), papers Selected from the 38th European Solid-State Device Research Conference – ESSDERC’08.
- [37] I. Gyongy, N. Calder, A. Davies, N. A. W. Dutton, R. R. Duncan, C. Rickman, P. Dalgarno, and R. K. Henderson, *IEEE Transactions on Electron Devices* **65**, 547 (2018).
- [38] J. Richardson, R. Walker, L. Grant, D. Stoppa, F. Borghetti, E. Charbon, M. Gersbach, and R. K. Henderson, in *2009 IEEE Custom Integrated Circuits Conference* (2009) pp. 77–80.
- [39] K. Morimoto, A. Ardelean, M.-L. Wu, A. C. Ulku, I. M. Antolovic, C. Bruschini, and E. Charbon, *Optica* **7**, 346 (2020).
- [40] In addition to fast imaging, individual atom addressing with single qubit rotations would be needed to optimize the enhanced survival probability from adaptive detection on an array of atoms.